LANGMUIR

pubs.acs.org/Langmuir Article

Gap-Dependent Surface-Enhanced Raman Scattering (SERS) Enhancement Model of SERS Substrate–Probe Combination Using a Polyelectrolyte Nanodroplet as a Distance Controller

Kullavadee Karn-orachai*

Cite This: *Langmuir* 2021, 37, 10776–10785

Read Online

ACCESS | Metrics & More | Article Recommendations | Supporting Information

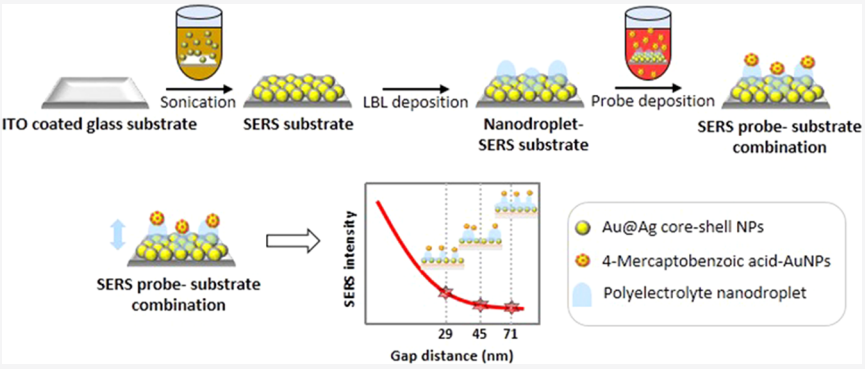

ABSTRACT: The development of surface-enhanced Raman scattering (SERS) biosensor platforms based on the sandwich combination of an SERS substrate and Raman reporter coated gold nanoparticle (AuNP) labeled with antibody has been widely performed for highly sensitive detection of biomolecules. The size of biomolecules located between these SERS-active materials dictates the sensitivity enhancement of the sensor. However, no suitable molecular size is provided. In this study, we report the gap-dependent SERS enhancement model using the combination of two SERS-active materials of 2D arrays of gold core–silver shell nanoparticles (Au@Ag core–shell NPs) as SERS-active substrates and mercaptobenzoic acid (MBA)-labeled AuNPs as SERS probes. The distance between these two materials is finely tuned using layer-by-layer assembled polyelectrolyte multilayer films. The morphology of the polyelectrolyte spacer is controlled into a droplet nanostructure, which is assumed to have a comparable shape with globular biomolecules. The well-controlled height or thickness of polyelectrolyte nanodroplet was achieved by changing number of deposition cycles. By increasing the thickness of the polyelectrolyte nanodroplet, MBA SERS intensities gradually decreased until at 40 nm-thick nanodroplet film and maintained afterward. This spacer thickness defined the limit of plasmonic coupling effect from this SERS probe–substrate combination. The SERS enhancement capability of this model was compared to conventional SERS immunoassay using three different antigen–antibody complex sizes of prostate-specific antigen, carcinoembryonic antigen, and carbohydrate antigen 19-9. Good agreement of the limitation of plasmon coupling as a function of the distance between the SERS substrate–probe combination using this developed model and SERS immunoassay was found. The finding provides valuable guidelines for immune-system selection in SERS immunosensors based on SERS substrate–probe combination.

INTRODUCTION

Surface-enhanced Raman scattering (SERS) has been considered to be one of the most powerful vibrational techniques for the highly sensitive detection of biological or chemical molecules adsorbed on metal nanostructure substrates.[1−5] The SERS phenomenon was first discovered by Fleischman and coworkers who reported extraordinary Raman signals of pyridine molecules adsorbed on a rough silver electrode.[6] Then, two independent research groups of Van Duyne and Creighton proposed an explanation of SERS enhancement, which was affected by not only the large rough surface but also the electromagnetic field and plasmonic field from nanostructures. SERS enhancement could be explained by two SERS enhancement mechanisms of electromagnetic enhancement (EM)[7,8] and chemical enhancement (CM).[9] The EM mechanism, which is the main enhancement, originates from the oscillation of electrons in the metal conduction band when nanomaterials are

Received: June 9, 2021
Revised: August 19, 2021
Published: August 31, 2021

https://doi.org/10.1021/acs.langmuir.1c01556
Langmuir 2021, 37, 10776–10785

irradiated with proper excitation energy. The resultant oscillation generates a strong electromagnetic field around the nanoparticle surface so-called localized surface plasmon resonance (LSPR). The LSPR excitation depends on the absorption and scattering of resonant radiation, resulting in strong plasmonic field at the nanostructure surface.[10] The CM mechanism, which is a minor enhancement, relates to the charge transfer between Raman molecules and metal nanostructures. The coexistence of the EM and CM enhancements is enabled in significant amplification of Raman intensity of analytes. This mechanism preferably occurs when Raman molecules are directly adsorbed or closely located on the nanostructure surface.[11,12] The EM enhancement strongly relies on the distance of the target molecule and plasmonic materials. The relatively long-range effect of the EM mechanism allows analyte molecules to be adsorbed directly and further away from the surface in nanometer scale. This is a promising enhancement for practical applications, especially in biosensors and bio-imaging. It is well-known that the SERS intensity and sensitivity of biosensors decrease as a function of distance away from the plasmonic surface.[13] Therefore, to recognize the great sensitivity enhancement the understanding of gap distance effect should be realized.

The investigations of distance-dependent SERS enhancement have been widely reported by various approaches of distance controllers. For example, Masango et al. reported the distance-dependent characteristics of SERS signal of trimethylaluminum (TMA) on silver film-over-nanospheres (AgFONs) as a function of separation distance.[14] The spacer between TMA and the SERS substrate was controlled by depositing an Al_2O_3 layer on the AgFON substrate. The intensity of Al−CH_3 and C−H signals of the TMA molecule depended on short- and long-range distance spacer. In addition, the distance-dependent characteristics for SERS systems can also be observed by varying interparticle spacing between two metal nanoparticles (NPs), combination of metal NPs and metal film, and incorporation of metal NPs and metal NP arrays. When those materials are placed in close proximity, the plasmon coupling of their plasmon resonance can occur via near-field interaction.[15,16] The coupled NP-film platform has been used to investigate the sensitivity of plasmon coupling as a function of separation distance. Mock et al. used a flat polyelectrolyte film[17] and Hill et al. utilized an ultrathin molecule[18] as a spacer between gold nanoparticles (AuNPs) and the Au film substrates to reveal the interplay between LSPR of AuNPs and that the surface plasmon polariton of Au film was sensitive to the separation distance. Nguyen et al. and Reinhard et al. reported the distance-dependence of metal nanoparticles pairing with different spacers of DNA.[19,20] The significant blue shift of the plasmon resonance peak and the decrease of SERS intensity indicated the lowering of plasmon coupling between AuNPs at the long separation distance.[21−23] Moreover, the sensitivity of SERS immunosensors changed when the distance between two plasmonic nanomaterials was varied. Nguyen et al. utilized Fab segment and whole antibody to control the distance between the SERS substrate and SERS tags to confirm the reduction of sensitivity as antibody length increased.[24] In addition, Karn-orachai et al. investigated the increment of SERS immunosensor sensitivity enhancement by using small antigen−antibody complexes compared to those of large molecular sizes.[25] These studies revealed useful information for choosing suitable sizes of biomolecules in SERS detection. However, the limitation of SERS enhancement in each report was quite different because of the variation of metal types, shapes, and metal compositions, and Raman measurement conditions. Although, various models for distance-dependent SERS enhancement have been widely investigated. Only continuous thin films of distance controlled over flat and nanostructured substrates were fabricated, whose morphology was unlike the globular shape of biomaterials. The plasmon coupling effect with respect to the separation distance of both platforms cannot be directly compared. However, the direct comparison of plasmon coupling efficiency regarding the globular-shaped gap spacer from the model and real immunosensor has not been investigated.

In this study, the model for investigation of the plasmon coupling efficiency as a function of separation distance between the SERS substrate and the probe was studied. A polymer multilayer film was created as a tunable spacer between the SERS substrate−probe combination. The morphology of this polymer film was controlled to be nanodroplet structure because this structure was designed to mimic the globular morphology of the antigen−antibody complex. The fabrication of polyelectrolyte nanodroplet arrays was achieved by introducing the conventional layer-by-layer (LbL) assembly of the positively charged polyallylamine hydrochloride (PAH) and negatively charged polyacrylic acid (PAA) at a certain concentration on the SERS-active substrate (2D arrays of gold core−silver shell (Au@Ag core−shell NPs)). The gap spacer between the SERS substrate−probe combination could be precisely controlled by varying the thickness of the nanodroplet of polyelectrolyte multilayers. The polyelectrolyte-deposited SERS substrates could be applied in this study because no peak interferes with the Raman signals of the Raman reporter molecules.[26] The SERS probes were the AuNPs labeled with mercaptobenzoic acid (MBA), which are negatively charged particles. The self-assembled SERS probe could electrostatically adsorb on the PAH outermost layer of the SERS-active substrate. The decrease of SERS intensity as a function of the separation distance between the SERS substrate and the probe was related to the decrease of plasmon coupling strength between the substrate and the probes. This work presents experimental results of a novel design to investigate the potential limits of SERS enhancement in the combination of SERS substrates and the probe. It is believed that this nanodroplet structure of polyelectrolyte film on the substrates would mimic the morphology of biomolecules deposited on that substrate in SERS biosensor systems.[27] Moreover, the SERS immunosensors with three different sizes of antigen−antibody complexes of prostate-specific antigen (PSA), carcinoembryonic antigen (CEA), and carbohydrate antigen 19−9 (CA 19−9) were also performed to compare the plasmon coupling efficiency. It was found that the sensitivity enhancement decreases as the molecular size of antigen−antibody complexes increased. This finding can be used as a comparative model with the SERS-based immunosensor for the prediction of the sensitivity enhancement at a certain spacer distance and it is useful for selecting the size of antigen/antibody in SERS immunosensors.

EXPERIMENTAL SECTION

Chemicals. Chloroauric acid ($HAuCl_4{\cdot}3H_2O$), MBA, 16-mercaptohexadecanoic acid (MHDA), PAA (Mw 1.8 kDa), PAH (Mw 56 kDa), poly (dimethyl diallyl ammonium chloride) (PDADMAC, Mw ≈ 400−500 kDa, 20% in H_2O), silver nitrate ($AgNO_3$), sodium citrate, ascorbic acid, dodecanethiol, octadecanethiol, (3-mercaptopropyl) trimethoxysilane (MPTMS, 98%), sodium chloride (NaCl), potassium chloride (KCl), sodium phosphate dibasic (Na_2HPO_4), and potassium

https://doi.org/10.1021/acs.langmuir.1c01556
Langmuir 2021, 37, 10776−10785

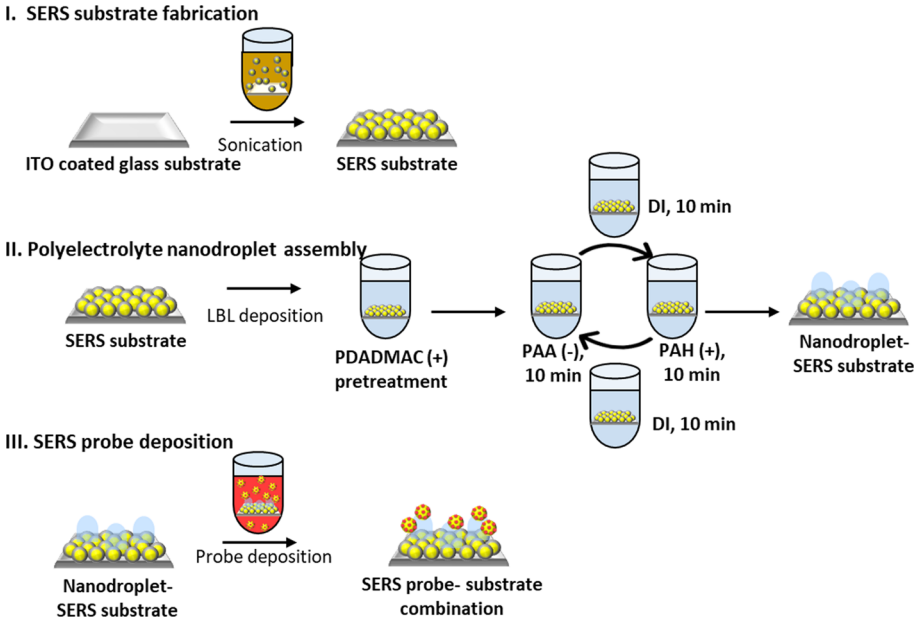

Figure 1. Fabrication process of the SERS probe−substrate combination consisting of three steps: (I) SERS substrate fabrication, (II) nanodroplet LbL assembly on SERS substrates, and (III) SERS probe deposition.

phosphate monobasic (KH_2PO_4), 1-ethyl-3[3-dimethylaminopropyl]-carbodiimide hydrochloride (EDC), *N*-hydroxysuccinimide (NHS), and bovine serum albumin (BSA) were obtained from Sigma-Aldrich. Toluene and acetone were purchased from Carlo Erba. The immunocomplex of PSA was obtained from Anogen and consisted of PSA monoclonal capture antibody (MO-T40081A), PSA monoclonal capture antibody (MO-T40081B), and PSA antigen (EL05−3). The immunocomplex of CEA provided from Anogen comprises CEA monoclonal capture antibody (MO-T40051A), CEA monoclonal detection antibody (MO-T40051B), and CEA antigen (MA1009). The immunocomplex of CA 19−9 received from Fitgeraldz comprises CA 19−9 monoclonal capture antibody (10-CA19A, clone M201214), CA 19−9 monoclonal detection antibody (10-CA19B, clone M201213), and CA 19−9 antigen (30-AC14) All chemicals and solvents were used as received without further purification. Distilled water (18.2 MΩ. cm) was used in all experiments.

Fabrication of the SERS Substrate−Probe Combination. The SERS substrate−probe combination was fabricated in three steps: (I) SERS substrate fabrication, (II) formation of polyelectrolyte nanodroplet on SERS substrates by LbL assembly, and (III) SERS probe deposition. Each fabrication step was explained separately as follows and a schematic illustration of each step is provided in Figure 1.

SERS Substrate Fabrication. A commercial 310−370 nm-thick indium tin oxide (ITO) sputtered-glass substrate (50 × 50 × 0.7 mm^3, Lumtec, Luminescence Technology Corp (Lot No.G002-160325006)) was chosen as a solid supporter for further SERS substrate fabrication. The ITO substrates were cut into square pieces of ∼1 × 1 cm^2. The substrates were sonicated in acetone and washed with deionized (DI) water thoroughly followed by drying under nitrogen. The substrates were thiolated by immersing in 1% v/v MPTMS in toluene for 24 h, washed with methanol three times, and finally dried under nitrogen blow. These thiolated ITO substrates were used for further arraying of Au@Ag core−shell NPs by a sonication method.[28]

The sodium citrate-capped 40 nm Au core and 5 nm Ag shell nanoparticles were synthesized by a seed-mediated growth method.[29,30] The morphology and EDS mapping images of Au@Ag core−shell NPs are shown in Figure S1. The Au@Ag core−shell NPs were capped with a mixture of dodecanethiol and octadecanethiol (6:1 molar ratio). These thiolated nanoparticles were dispersed in 2 mL of a 4:1 v/v mixture of hexane and acetone. The details of the synthesis are shown in ref 25. The solution was used to fabricate 2D arrays of Au@Ag core−shell NPs on the ITO substrate by using a sonication method with a minor modification.[27] The ultrasonic bath obtained from Elmasonic S 30 H was used in the fabrication of this 2D array. The dried Au@Ag core−shell NP powder (obtained from 30 mL of Au@Ag core−shell NP colloid) was re-dispersed in 1 mL of *n*-hexane in a glass vial (inner diameter = 2.3 cm) by sonication for several seconds. The MPTMS-treated ITO substrate was put in the resultant dark brown suspension, sonicated for 2 s and left for 2 s. The same steps were repeated 10 times. After the previous sonication step, the substrate was kept immersed in the suspension for 5 min, and then was moved to immerse in another glass vial containing 1 mL of n-hexane followed by a second sonication step for 10 s. Finally, a monolayer of Au@Ag core−shell NP arrays on the ITO substrate was achieved. After the deposition process, the 2D array samples were annealed at 60 °C overnight to introduce the chemisorption of the Au-S bond. The substrates were kept under a nitrogen box until further measurement.

Polyelectrolyte Nanodroplet Assembly on Substrates. In this study, two kinds of substrates were utilized including Au film and SERS substrates. Au film substrates were used as SERS-inactive materials, whereas, Au@Ag core−shell NP arrays served as SERS-active substrates. Before polymer deposition, these substrates were functionalized with 15 mM MHDA in ethanol solution at 50 °C for 12 h to introduce COOH ending groups at the outermost layer. To fabricate a certain barrier between the SERS substrate and the SERS probe, a sequential LbL deposition was performed based on our previous report.[31] The MHDA-treated substrates were immersed in PDADMAC solution (0.5 mg/mL, pH 6.0) for 10 min to introduce enough charges on the substrates and the excess amount of polymer was washed by immersing substrates into DI water under vigorous stirring for 10 min. This substrate was soaked in PAA solution (0.5 mg/mL, pH 6) for 10 min and then washed with DI water for 10 min to remove the excess PAH on the surface. After that, the sample was subjected to PAH solution (0.5 mg/mL, pH 3.5) for 10 min and washed with DI water while stirring for 10 min (Figure 1). This step resulted in a single bilayer or $(PAA/PAH)_{n=1}$ film. The deposition cycle was done alternately between PAA and PAH until the desired thickness was obtained and the substrate surface was covered with the positively charged PAH outermost layer. The thickness of the polymers was measured from dried samples using atomic force microscopy.

SERS Probe Deposition. First, 51 nm AuNPs were synthesized by a seed-growth mediation method.[25] Briefly, Au seeds (13 nm in diameter) were synthesized by reducing 20 mL of 0.5 mM $HAuCl_4$ with 1 mL of 38.8 mM sodium citrate and continued in boiling solution at 100 °C for 30 min to complete the reaction.[29] Then, 51 nm AuNPs were synthesized by adding 0.6 mL of Au seed colloid into 34 mL of

https://doi.org/10.1021/acs.langmuir.1c01556
Langmuir 2021, 37, 10776−10785

deionized water in a vessel under constant stirring. After that, 0.8 mL of 20 mM $HAuCl_4$ solution was added and subsequently 80 μL of 10 mM $AgNO_3$ solution was added. The solution was mixed for a few minutes and finally, the ascorbic acid solution was added with a constant feeding rate of 0.61 mL/min.[29] The solution was continuously stirred for 5 min after the ascorbic acid solution was added to complete the reduction process. These AuNPs served as supporting material for Raman reporter molecule functionalization. MBA was chosen to be a Raman reporter. 8 μL of 1 mM MBA in ethanol solution was mixed with 1 mL of Au colloid with optical density adjusted to unity under vigorous stirring for 3 h at room temperature. The excess amount of MBA was removed by two cycles of centrifugation at 6000 rpm for 5 min. Hereafter, the MBA-AuNPs were called SERS probes.

Since the polyelectrolyte-coated SERS substrates and SERS probe possessed positively and negatively charged nanomaterials, the SERS substrate−probe combination was created by electrostatic attraction. The corresponding substrates were immersed in SERS probe colloid (absorbance at 548 nm, optical density = 2) for 30 min. Then, the substrates were washed three times by rinsing with DI water and dried under nitrogen blow. After this step, the SERS substrate−probe combination was obtained. Figure 1 shows the fabrication process of the SERS substrate−probe combination in this study.

Sandwich Immunoassay Protocol for PSA, CEA, and CA 19−9 Detections. The sandwich immunoassays for PSA, CEA, and CA 19−9 detections were performed on the SERS substrates and Au film substrates (reference substrates). The sandwich immunoassay protocol was adapted from our previous report with minor modification.[25] Before the immunoassay step, the MHDA-treated SERS and Au film substrates were reacted with a mixed 15 mM EDC/NHS solution (1:1 v/v ratio) in a dark chamber for 30 min. The reaction was washed using PBS solution for three cycles. In the immunoassay for all systems, 20 μL of 1 μg/mL of capture antibody was dropped on the substrates and incubated overnight at room temperature. Then, unbound antibodies were washed by phosphate buffer saline solution (10 mM PBS, pH 7.4) three times. The nonspecific binding sites were blocked with BSA, which was conducted by immersing the substrates in a PBS solution with 0.05% (w/v) BSA for 30 min. The free BSAs were removed by rinsing with PBS solution. The immunosubstrates were stored in a PBS solution at 4 °C until being used. The antigen immobilization was performed by dropping 20 μL of antigen solution onto the immunosubstrates and kept in a moist chamber at RT for 20 min. The unbound antigen was removed by rinsing with PBS solution. Next, 20 μL of SERS probes conjugated with detection antibody was pipetted onto the immunosubstrates, and the solution was kept on the substrates for 30 min to complete the antigen−antibody binding. To remove unreacted SERS probes, the substrates were rinsed sequentially with PBS solution, and DI water and dried under N_2 gas flow. Finally, the Raman spectra of the samples were acquired.

Characterization. Scanning electron microscopy (SEM SU8230, Hitachi) was used to examine the morphology and coverage of particles on the samples. A UV−vis spectrophotometer (Lambda 650, Perkin Elmer) was used to observe the optical property of the samples. UV−vis spectra in the wavelength range of 300 to 800 nm were recorded with a scanning step of 0.5 nm. Raman spectra of the SERS probe were collected by a Raman spectrometer with a He-Ne laser (633 nm) and charge-coupled device detector (NT-MDT NTEGRA spectra). The 633 nm excitation laser was focused on the substrate surface by a 40× objective lens with a numerical aperture of 0.65 and the laser power at the sample surface was 100 μW. Raman shift spectra in the range of 300−2000 cm^{-1} were obtained with 10 s acquisition time. Typically, five spectra were averaged to improve the signal-to-noise ratio. For Raman mapping measurement, 100× objective lens (NA 0.85) was used to focus the laser on the sample surface. The Raman mapping image was built by integrating the major Raman signal of MBA at 1080 cm^{-1} from 50 × 50 μm^2 analysis area of point-by-point scanning. The exposure time was fixed to 1 s and resolution of mapping image was 64 × 64 pixels. Moreover, atomic force microscopy (AFM 5300E, Hitachi) was used to determine polymer thicknesses. The standard dynamic tapping mode was conducted under vacuum by using a cantilever with a spring constant of 33 N m^{-1}. The resolution of images was fixed at 512 × 512 and the scan rate was 0.3 Hz.

RESULTS AND DISCUSSION

Optimization of Concentrations of Polyelectrolytes. The concentration of polyelectrolyte solution is a crucial factor for nanodroplet polyelectrolyte multilayer (PEM) film formation on SERS substrates. In this study, the concentration of PDADMAC, PAA, and PAH was varied in the range of 0.5 to 2 mg/mL. The polymers were deposited for 9 to 33 bilayers for investigating the concentration effect as a function of polymer thickness. After the drying process, these polymer-coated substrates were characterized using SEM to investigate the morphology of the polymer on SERS substrates. Figure 2 shows

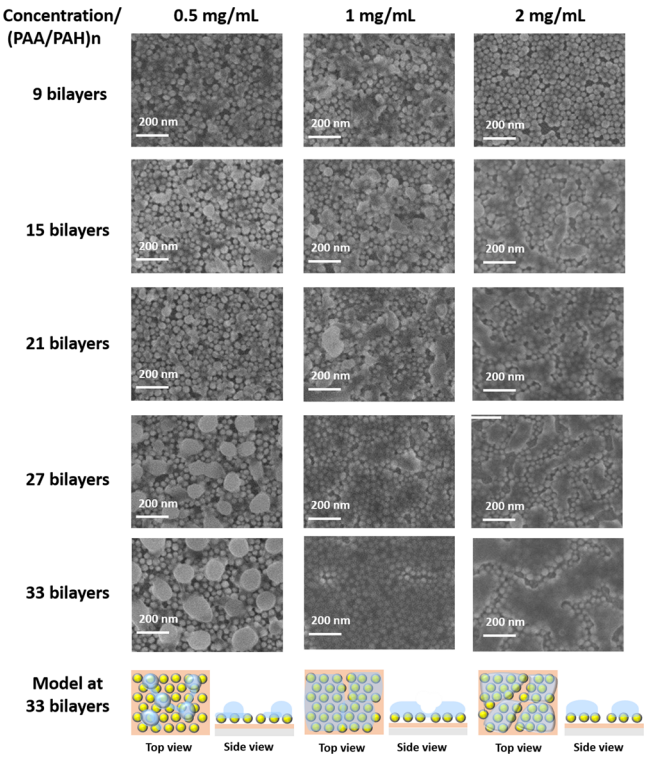

Figure 2. SEM images of $(PAA/PAH)_{9-33}$ film deposited on SERS substrates with different concentrations of polyelectrolytes. Schematic illustration of polymer films with three polymer concentrations at 33 bilayers on SERS substrates.

SEM images of the $(PAA/PAH)_{n=9-33}$ film deposited on SERS substrates with different concentrations of polyelectrolytes. It was found that the morphology of thin $(PAA/PAH)_{n<20}$ films on SERS substrates with three different polyelectrolyte concentrations appeared almost the same. It showed non-contiguous polymer nanodroplets and cobweb-like structures on the substrates as seen in the growth of polymer film on the SERS substrates in SEM images. These structures were originated from dewetting of liquid polyelectrolyte solution on the SERS substrates.[32] On the other hand, the morphology variation of thicker $(PAA/PAH)_{n>20}$ films was observed. The nanodroplet structure of the polyelectrolyte concentration of 0.5 mg/mL and continuous film with cracks or coalesced droplets at higher concentrations of polyelectrolytes (1 and 2 mg/mL). For a low polyelectrolyte concentration of 0.5 mg/mL, the nucleation of the nanodroplet in an early stage $(PAA/PAH)_{n<20}$ of deposition was formed, resulting from spinodal dewetting.[32]

https://doi.org/10.1021/acs.langmuir.1c01556
Langmuir 2021, 37, 10776−10785

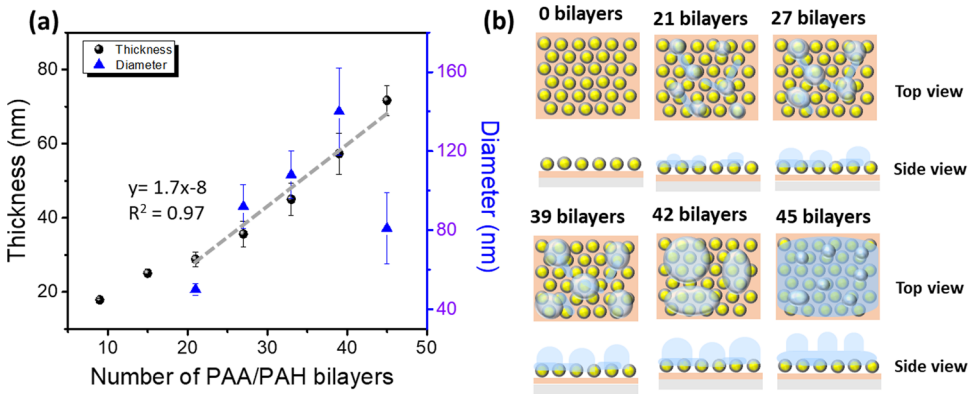

Figure 3. (a) Plot with double *y*-axes: thickness (on the left) and diameter of nanodroplet (on the right) versus the number of PAA/PAH bilayers. Dashed line represents the linear range from 21 to 45 bilayers with R^2 of 0.97. (b) Growth model of polyelectrolyte nanodroplet on the SERS substrate.

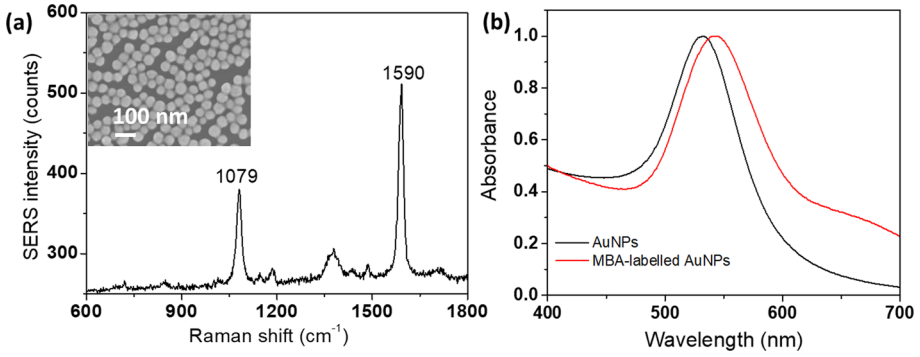

Figure 4. (a) Raman spectrum of MBA-AuNPs. Inset shows a SEM image of the corresponding AuNPs having 51 ± 4 nm average diameter. (b) Extinction spectra of the as-prepared AuNPs and MBA-labeled AuNPs.

These nanodroplets served as templates for further alternate adsorption of oppositely charged polyelectrolytes to finally produce larger nanodroplets on the SERS substrates. The dewetting behavior occurred promptly at this condition, which was in good agreement with previous reports. The higher polyelectrolyte concentrations (1, 2 mg/mL) gave relatively flat thin films, unlike the low concentration of 0.5 mg/mL. The schematic of polymer film formation at different polyelectrolyte concentrations and numbers of (PAA/PAH) bilayers is shown in Figure 2.

In addition, the formation of polyelectrolytes nanodroplets was performed on both SERS and Au film substrates to compare the effect of roughness of the substrates. The thick $(PAA/PAH)_{n=33}$ films were used to compare nanodroplet morphology on both substrates because the nanostructure was observed. It was found that the morphology of $(PAA/PAH)_{n\,=\,33}$ film on both SERS and Au film substrates was the same as those shown in Figure 2 and S2, respectively. It was confirmed that the dewetting behavior of polyelectrolytes took place on both nanorough and flat substrates. In comparison to all PEM structures on substrates, $(PAA/PAH)_n$ films at the concentration of 0.5 mg/mL showed interesting nanostructures. This nanodroplet polyelectrolyte was easily built up by an alternate dip-coating method. Polyelectrolyte dewetting enabled to produce a large area of uniform nanodroplets on the substrates. Therefore, this condition was chosen to further study in more detail.

Physical Properties of Polyelectrolytes Nanodroplets at a Concentration of 0.5 mg/mL on SERS Substrates. The characteristics of polyelectrolytes nanodroplet films including morphology, thickness, and diameter of nanodroplet were investigated from dried polymer films on SERS substrates using AFM and SEM. The evolution of polymer nanodroplet thickness and diameter as a function of the number of PAA/PAH bilayers was studied. The SEM images of the entire fabrication of polyelectrolyte nanodroplet on SERS substrates at 0 to 45 bilayers are provided in Figure S3. The diameter and height of isolated nanodroplets were gradually increased as the increment of deposition cycles (Figure S3). Interestingly, the diameter of nanodroplets was decreased again after the deposition cycle increased up to 45 bilayers. This is because the new small nanodroplets were built up again on the continuous film with cracks at 42 bilayers of the PAA/PAH film (Figure S3). Moreover, the particle size distribution of the polyelectrolyte nanodroplet at 21 to 45 bilayers was also analyzed from 100 different droplet nanostructures from SEM images. Figure S4 reveals the histogram of size distributions of polyelectrolyte nanodroplets at 21 to 45 bilayers on the SERS substrates. It was found that the nanodroplets were not entirely uniform for all thicknesses of polyelectrolyte nanodroplets. The uniform polyelectrolyte nanodroplets with narrow size distribution were found for 21 and 45 bilayers, which have a small particle size. However, the increment of deposition cycles (27 to 39 bilayers) gave a broad size distribution of polyelectrolyte nanodroplets.

Figure 3(a) exhibits the double y-axes: thickness (on the left) and diameter of nanodroplet (on the right) versus numbers of PAA/PAH bilayers. The thickness and diameter of each droplet were estimated from AFM and SEM images, respectively. The AFM topography and height profile images of polyelectrolyte

https://doi.org/10.1021/acs.langmuir.1c01556
Langmuir 2021, 37, 10776−10785

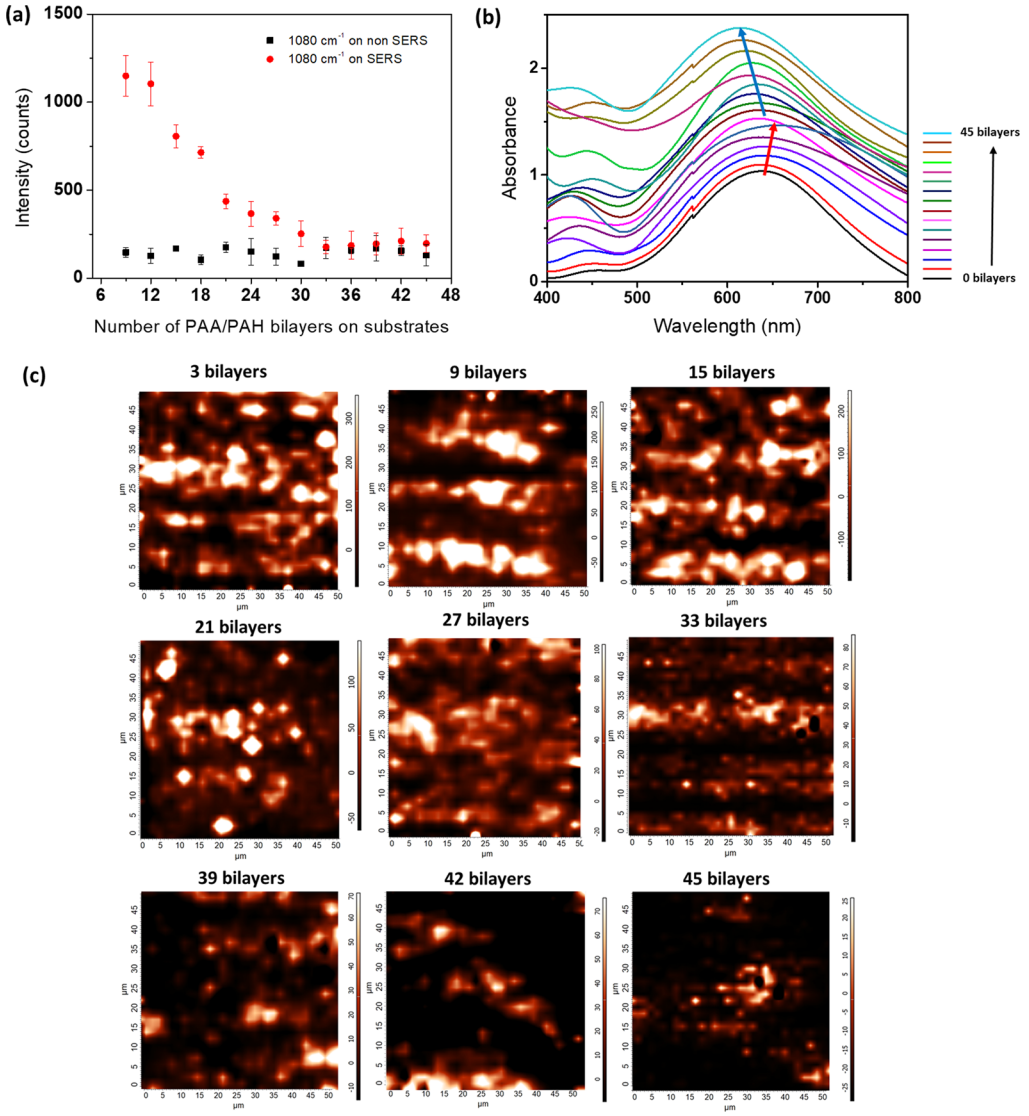

Figure 5. (a) Relationships between the averaged intensity of Raman signals of SERS probe and numbers of PAA/PAH bilayers on non-SERS substrate: Au film (■ at 1080 cm^{-1}) and SERS substrate (● at 1080 cm^{-1}). (b) Extinction spectra of SERS substrate−probe combination at different numbers of PAA/PAH bilayers. (c) 2D distribution of hotspot localization of the SERS substrate−probe combination at different numbers of PAA/PAH bilayers.

nanodroplet-coated SERS substrates are shown in Figure S5. The diameter and height of nanodroplets were averaged from 50 different nanodroplets. Since the nanodroplet structure was observed from 21 to 45 bilayers, the characteristics diameters of the $(PAA/PAH)_{n\ =\ 21-45}$ film were plotted as a function of numbers of (PAA/PAH) bilayers. The linear relationship between thickness and the number of PAA/PAH bilayers was in the range of 21 to 45 PAA/PAH bilayers, which was fitted as $y = 1.7x - 8$, $R^2 = 0.97$. The increment of thickness corresponds to the molecular arrangement of the polymer chain on the substrate. The thickness of PDADMAC pretreatment was also included in the obtained thickness from AFM image analysis. According to the thickness result from linear regression, the average thickness of one bilayer was determined to be 1.7 ± 0.4 nm. In addition, the measured diameter of polyelectrolyte nanodroplets increased as the number of deposition steps increased from 21 to 39 bilayers and decreased at 45 bilayers. Illustrations shown in Figure 3(b) represent top and side views of the growth model of these polyelectrolytes nanodroplet films on SERS substrates, respectively. Because of the advantages of the LbL process being easy and offering precise control of the film thickness, this method was chosen to make a controllable surface barrier between SERS-active substrate and the probe by varying the number of deposited PAA/PAH bilayers on the SERS-active substrate.

Characterization of SERS Probe. The physical properties of the SERS probe were characterized by SEM and Raman spectroscopy. Figure 4(a) shows the Raman spectra of AuNPs labeled with MBA. The characteristic Raman peaks of MBA-labeled AuNPs were found at 1079 and 1587 cm^{-1}, which corresponded to benzene ring breathing and C═C ring vibration mode, respectively.[33−35] These intense peaks were used to determine the plasmon coupling efficiency between the SERS substrate and the probe when the spacer distance was varied. The SEM image of the SERS probe is shown in Figure 4(a, inset). They were spherical with a uniform size of 51 ± 4 nm average diameter. The extinction spectra of 51-nm-AuNPs and MBA-labeled AuNPs are shown in Figure 4(b). The maximum plasmon band attributed to the LSPR of bare AuNPs, and SERS probe was located at 532, and 543 nm, respectively. A redshift of

https://doi.org/10.1021/acs.langmuir.1c01556
Langmuir 2021, 37, 10776−10785

LSPR was found after deposited MBA molecules on AuNPs through Au-S linkage because of a change of the refractive index in the AuNP colloids.

Dependence of SERS Enhancement on the Distance Separation between the SERS Substrate and the Probe. It has been reported that the strength of the electromagnetic field produced from the substrate decreases with increasing distance away from the surface.[17,20,21] To explain this phenomenon, it was hypothesized that polyelectrolyte nanodroplets dictated the gap size, thereby controlling the SERS signal and enhancement. The distance between the SERS substrate and the probe was controlled by changing the thickness of the polyelectrolyte nanodroplet structure to fine-tune the strength of plasmon coupling between those SERS-active materials. The SERS probe directly situated on the polyelectrolyte nanodroplet-coated SERS substrate via electrostatic attraction force. The SERS probe-polyelectrolyte nanodroplet-coated SERS substrate system so-called SERS substrate−probe combination was constructed. To have different spacers, the thickness of polyelectrolyte nanodroplet was adjusted in the range of 17 to 71 nm, which corresponded to 9 to 45 PAA/PAH bilayers. Raman spectroscopy, UV−vis spectrometer, and SEM were conducted to investigate the properties of this model. Polyelectrolyte-coated SERS substrates had no interference signal, which did not change both Raman signals as seen in the similar pattern of SERS spectra from both SERS substrate−probe combination and individual SERS probe (Figure S6). Moreover, the MBA intensity from SERS substrate−probe combination was much higher than that from only the SERS probe because SERS substrate−probe combination provides strong electromagnetic field enhancement to emphasize the MBA signal.

Before determination of the plasmon coupling efficiency as a function of separation distance from the SERS-active substrates, a similar experiment was also performed on a flat Au film as a reference. The SERS probe was coated on polyelectrolyte nanodroplet-coated SERS and Au film using different PAA/PAH bilayers from 3 to 45 bilayers. The Raman signal of MBA on both SERS and Au film substrates was monitored and compared. The representative SERS spectra on both SERS and Au substrates are shown in Figure S7. The corresponding SEM images of SERS substrate−probe combination at different thicknesses of polyelectrolyte layers are shown in Figure S8. Figure 5(a) shows a plot between MBA intensities at 1080 cm^{-1} against the number of PAA/PAH bilayers, which represents the distance separation between the SERS probe and substrates. For the reference system (Au film), the Raman intensities at 1080 cm^{-1} of the SERS probe deposited on PAA/PAH bilayer treated Au film were not varied with the change of polymer thickness. It indicates that no influence of the separation distance on the intensity of SERS probe-Au substrate combination. In the case of SERS substrate−probe combination, the intensity of MBA was gradually decreased with increasing number of PAA/PAH bilayers. The strong electromagnetic field coupling between the SERS probe and the SERS substrate occurred when a small number of PAA/PAH bilayers was deposited as intense MBA intensity. The less plasmonic coupling between the SERS probe and the SERS substrate was found by observing low MBA signal when thick polymer nanodroplet was used as a barrier on the SERS substrate. The SERS intensity of MBA molecules trailed off at 33 (PAA/PAH) bilayers (45 nm), which defined the limits of plasmon coupling efficiency from this combined SERS substrate and probe. After the distance separation was over 45 nm, no coupling or fewer SERS-enhancing effects were found because of too far distance. Our findings showed the same trend as previous reports that studied the SERS intensity reduction of metal nanoparticle pairs against separation distance controlled by DNA.[19,20] However, the limitation of plasmon length obtained from this study was different from other reports because of the different SERS systems including particle size of AuNPs, type of Raman reporter molecule, and detection conditions.

The evidence to confirm the plasmonic coupling in the SERS substrate−probe combination was revealed by monitoring the plasmon shift as a function of the number of PAA/PAH bilayers using UV−vis spectroscopy. To confirm that the plasmon shift comes from the increment of separation distance, extinction spectra of the as-prepared, and polyelectrolyte-coated SERS substrates were measured. Both substrates gave comparable spectra with the same absorption maxima at 638 nm (Figure S9), indicating that polyelectrolyte nanodroplet does not affect the plasmon resonance of SERS substrate. After SERS substrate−probe combination was fabricated, plasmon resonance interaction was monitored by investigating the LSPR wavelength shift of the SERS substrate. As our substrate comprising of Au@AgNPs arrays, polyelectrolyte layer, and SERS probes, the absorption peak of this substrate would affect by the plasmon resonance of both SERS substrate and probe. Therefore, the detected spectra will be the superposition of both components with various separation distances. Figure 5(b) shows the extinction spectra of SERS substrate−probe combination at various thicknesses of polyelectrolyte nanodroplets. As the thickness of polyelectrolyte nanodroplet increased from 0 to 15 bilayers, the LSPR of SERS substrate slightly shifted to longer wavelength (from 638 to 651 nm). It is caused by the strong plasmon coupling between SERS substrate and probe. This behavior was also found by Wu and coworkers.[36] They observed the coupling of plasmon oscillation of two adjacent AuNPs via near-field interaction, which showed that LSPR shifted to longer wavelength comparing with the LSPR of individual AuNPs. The LSPR of SERS substrate−probe combination having $(PAA/PAH)_{n = 18-33}$ films was slightly redshifted from 651 to 633 nm, indicating the reduction of plasmon coupling between the SERS substrate and probe regarding the separation distance between the SERS substrate and probe.[37] Then, a large blue shift to ∼614 nm in plasmon band of SERS substrates was induced after increase of number of PAA/PAH films from 36 to 45 bilayers. The thick distance controller could conceal the electromagnetic coupling. Zeng and coworkers have reported the blue shift of plasmon resonance of Au nanodiscs (75 nm in diameter) when the interparticle spacing between nanodiscs was fixed from 35 to 160 nm. The blue-shift LSPR of Au nanodiscs is caused by the generation of bonding and antibonding from LSPR hybridization and electrostatic repulsion force.[38] The trend was consistent with that observed exponential reduction of MBA signal from Raman measurement. Owing to the nature of electromagnetic near-field concentration at the SERS substrate surface, the limitation of plasmon coupling was defined by the separation distance of polyelectrolyte nanodroplet.

Moreover, the electromagnetic field distribution of this system was proved by performing Raman mapping measurement. It is supposed that the enhancement efficiency of the SERS substrate will be predicted from the SERS hotspot localization on the SERS substrate. Raman measurement was performed using SERS substrate−probe combination under dried condition. The Raman mapping image shows the

https://doi.org/10.1021/acs.langmuir.1c01556
Langmuir 2021, 37, 10776−10785

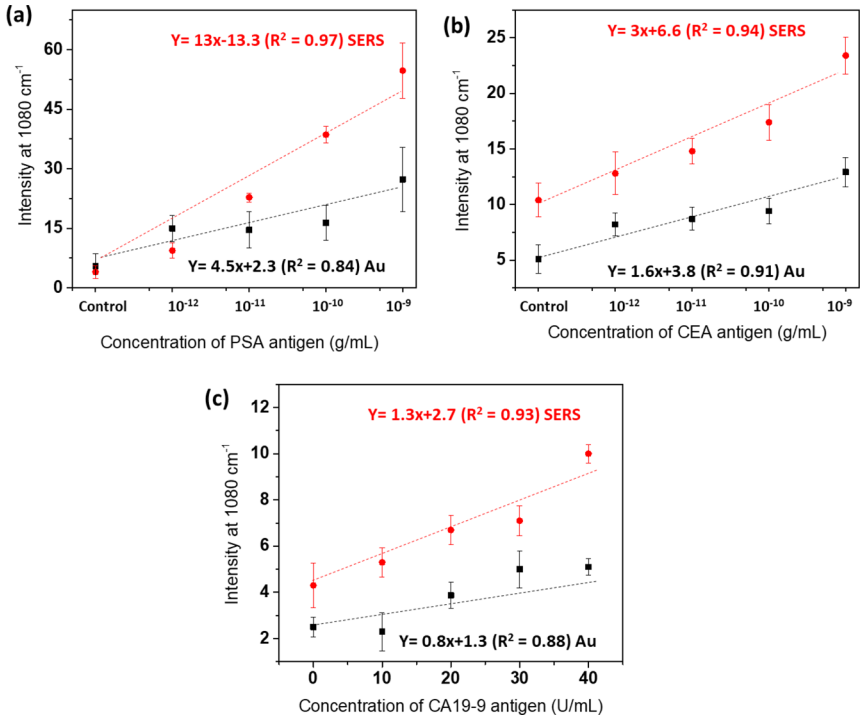

Figure 6. Sensitivity curves of sandwich-based SERS immunosensors for (a) PSA, (b) CEA, (c) and CA 19-9 performed on SERS (circle) and Au film substrates (square).Dashed lines are obtained by the method of least squares.

localization of strong and weak electromagnetic field regions of each model coated with different thicknesses of polyelectrolyte nanodroplet. The Raman signal at 1080 cm^{-1} of MBA molecule deposited on the SERS probe was used to track the hotspot region. Figure 5(c) illustrates the 2D distribution of hotspot localization of the SERS substrate−probe combination at different numbers of PAA/PAH bilayers. The bright region of the Raman mapping image corresponds to the SERS hotspot localization or high SERS intensity. The hotspot of this sample was generated by plasmon coupling of electromagnetic fields originated from both SERS substrate and probe. It was found that the hotspot density decreased with increasing numbers of PAA/PAH bilayers. The Raman signal of substrate−probe combination using thin PAA/PAH bilayers was more intense than that using thin PAA/PAH bilayers. This confirmed that the propagation of the electromagnetic field strongly depends on the separation distance.

Comparative Study of SERS Enhancement from Nanodroplet-Coated SERS Substrate and SERS Immunosensors at Certain Spacer Distances. To compare our findings to typical SERS immunosensors with different distance spacers between the SERS substrates and probes, sandwich antigen−antibody complexes with different molecular sizes were utilized for SERS immunosensor fabrication. Three types of sandwich antigen−antibody complexes with different sizes of antigen of PSA, CEA, and CA19−9 were selected to compare with the corresponding polyelectrolyte nanodroplet spacers at 21, 27, and 33 PAA/PAH bilayers. The distance spacer in SERS immunosensors was defined by the molecular size of each biomolecule in the sandwich complexes, which is assembled in the vertical axis of the capture antibody−antigen-detection antibody. The molecular size estimation of antigen−antibody complexes was calculated according to the previous report.[25] Typically, the intact antibody has a molecular weight of 150 kDa with approximately 13 nm length. The antigen for PSA, CEA, and CA 19−9 has a molecular weight of about 34, 180, and 210 kDa, which is assumed to have the molecular size of about 2.9, 15.6, and 18.2 nm in length, respectively. Therefore, the total size of sandwich immunocomplexes for PSA, CEA, and CA 19−9 is approximately about 28.9, 41.6, and 44.2 nm. The SERS enhancement obtained from the average thickness of nanodroplets at about 29, 41, and 45 nm from 21, 30, and 33 bilayers was selected to compare with the sensitivity enhancement obtained from SERS immunosensors. It was believed that the morphology of this polyelectrolyte nanodroplet and sandwich immunocomplexes was comparable since the structure of both nanodroplet and antigen−antibody complexes were assumed to have a globular shape.

The sensitivity study of SERS immunosensors of those selected antigen−antibody complexes was performed by measuring MBA signal on SERS probe after the final step of immunoassays. For sensitivity study, different concentrations of the PSA, CEA, and CA 19−9 antigens were prepared via serial dilution into a final concentration range of 1 ng/mL to 1 pg/mL for PSA and CEA systems and 10 to 40 unit (U)/mL for CA 19−9 immunoassay. This concentration range was selected to perform SERS immunosensors because it was slightly lower than the normal range at 4 ng/mL, 2.5−5 ng/mL, and 37 U/mL for PSA, CEA, and CA 19−9, respectively.[39−41]

The representative SERS spectra of PSA, CEA, and CA 19−9 immunoassay systems with different antigen concentrations on both SERS and Au film substrates are shown in Figure S10. The sensitivity curves were obtained by plotting the intensity of the 1080 cm^{-1} band as a function of the concentration of antigen protein. The sensitivity curves of PSA, CEA, and CA 19−9 immunoassay systems with different antigen concentrations on both SERS and Au film substrates are shown in Figure 6(a-c). The sensitivity enhancement of each immunoassay was calculated by the slope from SERS systems divided by the slope from the Au film system. It was found that the sensitivity

https://doi.org/10.1021/acs.langmuir.1c01556
Langmuir 2021, 37, 10776−10785

enhancement of PSA on SERS substrate was approximately three times higher than that on Au film substrate. Moreover, low sensitivity enhancement of about 2 and 1.6 times was achieved from CEA and CA 19-9 immunoassay, respectively, by comparing sensitivity from SERS and Au film system. As the size of immunocomplexes increased more than 40 nm, no significant SERS sensitivity amplification compared to the flat Au substrates was found. It indicates that the distance between the analyte and the SERS substrate is too large to produce enough SERS-enhancing effect. These findings proved that the sensitivity enhancement is strongly related to the size of immunocomplexes. Based on the discussion above, the combination of SERS substrate and the probe showed a good enhancement in the immunosensor application with biomolecular size up to 40 nm. However, the sensitivity enhancement from the immunoassay system could not be directly compared to the enhancement achieved from the model of the SERS substrate−probe combination. It was because the density of biomolecule and polyelectrolyte nanodroplet was not the same, which strongly affected the density of probe and SERS enhancement. Notwithstanding, a similar trend of less SERS enhancement and low sensitivity amplification was found at larger spacer (>40 nm) between the SERS probe and the substrate. These findings confirmed that the polyelectrolyte nanodroplet and biomolecular size in immunoassays dictate the gap size, which affected the SERS signal and enhancement.

CONCLUSIONS

The distance-dependence SERS enhancement model was successfully fabricated by electrostatic attraction force of three components including Au@Ag core−shell NP array substrate, polyelectrolyte nanodroplet, and MBA coated AuNPs. The polymer with droplet morphology was controlled by using a proper concentration of polyelectrolyte solution (0.5 mg/mL). The thickness of nanodroplet multilayers was tuned by varying alternate adsorption of oppositely charged polyelectrolytes. The polyelectrolyte nanodroplet was recognized as a well-controlled linker between two SERS-active materials for understanding the strength of plasmon coupling between those SERS-active materials. The distance-dependent SERS enhancement model was constructing through alternated electrostatic deposition of polyelectrolytes on charged SERS substrates followed by dipping in negatively charged SERS probe. By considering the relationship between MBA intensities of the SERS probe as a function of the number of PAA/PAH bilayers on the substrate, the SERS intensity gradually decreased with increasing separation distance (thickness of PAA/PAH bilayers) between the SERS probe and the substrate. The plasmon coupling was negligible when the distance separation between the probe and substrate was longer than 45 nm or 33 PAA/PAH bilayers. Moreover, the combination of the SERS substrate and probe was also used for demonstrating three types of sandwich immunoassays, which have an antigen size about 2.9, 15.6, and 18.2 nm for PSA, CEA, and CA 19−9, respectively. A sandwich immunoassay consists of two antibodies and one antigen, the total size of sandwich immunocomplexes for PSA, CEA, and CA 19−9 was about 28.9, 41.6, 44.2 nm, respectively. The highest SERS amplification was found when using the smallest antigen size (PSA system). The less sensitivity enhancement was obtained when the antigen−antibody complex size was larger than 40 nm, which showed good agreement of plasmon coupling capability as obtained from this developed model. This finding can be useful to explain the limitation of targeted biomaterial size that was applied between SERS probe-SERS substrate.

ASSOCIATED CONTENT

Supporting Information

The Supporting Information is available free of charge at https://pubs.acs.org/doi/10.1021/acs.langmuir.1c01556.

Morphology of Au@Ag core−shell NPs, morphology of polymer-coated Au film and the SERS substrate, size distribution of polyelectrolyte nanodroplets, Raman spectra of SERS probe and SERS substrate−probe combination, morphology of SERS substrate−probe combination at different thicknesses of polyelectrolyte layers, and Raman spectra of SERS immunosensors of PSA, CEA, CA 19−9 (PDF)

AUTHOR INFORMATION

Corresponding Author

Kullavadee Karn-orachai − *National Nanotechnology Center (NANOTEC), National Science and Technology Development Agency (NSTDA), Pathumthani 12120, Thailand;*
orcid.org/0000-0001-7912-5778;
Email: kullavadee.kar@nanotec.or.th

Complete contact information is available at:
https://pubs.acs.org/10.1021/acs.langmuir.1c01556

Notes

The author declares no competing financial interest.

ACKNOWLEDGMENTS

This research was supported by National Nanotechnology Center (NANOTEC, grant number P1850313, and P1851654), National Science and Technology Development Agency (NSTDA), Thailand. The fruitful discussion with Prof. Dr. Supapan Seraphin is acknowledged.

REFERENCES

(1) Shanmukh, S.; Jones, L.; Driskell, J.; Zhao, Y.; Dluhy, R.; Tripp, R. A. Rapid and Sensitive Detection of Respiratory Virus Molecular Signatures Using a Silver Nanorod Array SERS Substrate. *Nano Lett.* **2006**, *6*, 2630−2636.

(2) Kneipp, K.; Flemming, J. Surface enhanced Raman scattering (SERS) of nucleic acids adsrobed on colloidal silver particles. *J. Mol. Struct.* **1986**, *145*, 173−179.

(3) Gong, Z.; Du, H.; Cheng, F.; Wang, C.; Wang, C.; Fan, M. Fabrication of SERS Swab for Direct Detection of Trace Explosives in Fingerprints. *ACS Appl. Mater. Interfaces* **2014**, *6*, 21931−21937.

(4) Chen, J.; Huang, Y.; Kannan, P.; Zhang, L.; Lin, Z.; Zhang, J.; Chen, T.; Guo, L. Flexible and Adhesive Surface Enhance Raman Scattering Active Tape for Rapid Detection of Pesticide Residues in Fruits and Vegetables. *Anal. Chem.* **2016**, *88*, 2149−2155.

(5) Xu, H.; Bjerneld, E. J.; Käll, M.; Börjesson, L. Spectroscopy of Single Hemoglobin Molecules by Surface Enhanced Raman Scattering. *Phys. Rev. Lett.* **1999**, *83*, 4357−4360.

(6) Fleischmann, M.; Hendra, P. J.; McQuillan, A. J. Raman spectra of pyridine adsorbed at a silver electrode. *Chem. Phys. Lett.* **1974**, *26*, 163−166.

(7) Stiles, P. L.; Dieringer, J. A.; Shah, N. C.; Van Duyne, R. P. Surface enhanced Raman Spectroscopy. *Annu. Rev. Anal. Chem.* **2008**, *1*, 601−626.

(8) Lombardi, J. R.; Birke, R. L. A unified approach to surface-enhanced Raman spectroscopy. *J. Phys. Chem. C* **2008**, *112*, 5605−5617.

(9) Campion, A.; Ivanecky, J. E., III; Child, C. M.; Foster, M. On the mechanism of chemical enhancement in surface-enhanced Raman scattering. *J. Am. Chem. Soc.* **1995**, *117*, 11807−11808.
(10) Álvarez-Puebla, R. A. Effects of the Excitation Wavelength on the SERS Spectrum. *J. Phys. Chem. Lett.* **2012**, *3*, 857−866.
(11) Kim, K.; Shin, D.; Kim, K. L.; Shin, K. S. Electromagnetic field enhancement in the gap between two Au nanoparticles: the size of hot site probed by surface-enhanced Raman scattering. *Phys. Chem. Chem. Phys.* **2010**, *12*, 3747−3752.
(12) Qian, X.; Li, J.; Nie, S. Stimuli-Responsive SERS Nanoparticles: Conformational Control of Plasmonic Coupling and Surface Raman Enhancement. *J. Am. Chem. Soc.* **2009**, *131*, 7540−7541.
(13) Guo, L.; Jackman, J. A.; Yang, H.-H.; Chen, P.; Cho, N.-J.; Kim, D.-H. Strategies for enhancing the sensitivity of plasmonic nanosensors. *Nano Today* **2015**, *10*, 213−239.
(14) Masango, S. S.; Hackler, R. A.; Large, N.; Henry, A.-I.; McAnally, M. O.; Schatz, G. C.; Stair, P. C.; Van Duyne, R. P. High-Resolution Distance Dependence Study of Surface-Enhanced Raman Scattering Enabled by Atomic Layer Deposition. *Nano Lett.* **2016**, *16*, 4251−4259.
(15) Fromm, D. P.; Sundaramurthy, A.; Schuck, P. J.; Kino, G.; Moerner, W. E. Gap-Dependent Optical Coupling of Single "Bowtie" Nanoantennas Resonant in the Visible. *Nano Lett.* **2004**, *4*, 957−961.
(16) Nordlander, P.; Oubre, C.; Prodan, E.; Li, K.; Stockman, M. I. Plasmon Hybridization in Nanoparticle Dimers. *Nano Lett.* **2004**, *4*, 899−903.
(17) Mock, J. J.; Hill, R. T.; Degiron, A.; Zauscher, S.; Chilkoti, A.; Smith, D. R. Distance-Dependent Plasmon Resonant Coupling between a Gold Nanoparticle and Gold Film. *Nano Lett.* **2008**, *8*, 2245−2252.
(18) Hill, R. T.; Mock, J. J.; Hucknall, A.; Wolter, S. D.; Jokerst, N. M.; Smith, D. R.; Chilkoti, A. Plasmon Ruler with Ångstrom Length Resolution. *ACS Nano* **2012**, *6*, 9237−9246.
(19) Reinhard, B. M.; Siu, M.; Agarwal, H.; Alivisatos, A. P.; Liphardt, J. Calibration of Dynamic Molecular Rulers Based on Plasmon Coupling between Gold Nanoparticles. *Nano Lett.* **2005**, *5*, 2246−2252.
(20) Nguyen, A. H.; Lee, J. U.; Sim, S. J. Plasmonic coupling-dependent SERS of gold nanoparticles anchored on methylated DNA and detection of global DNA methylation in SERS-based platforms. *Aust. J. Optom.* **2015**, *17*, No. 114022.
(21) Su, K.-H.; Wei, Q.-H.; Zhang, X.; Mock, J. J.; Smith, D. R.; Schultz, S. Interparticle coupling effects on plasmon resonances of nanogold particles. *Nano Lett.* **2003**, *3*, 1087−1090.
(22) Park, T. J.; Lee, S. J.; Kim, D.-K.; Heo, N. S.; Park, J. Y.; Lee, S. Y. Development of label-free optical diagnosis for sensitive detection of influenza virus with genetically engineered fusion protein. *Talanta* **2012**, *89*, 246−252.
(23) Lin, Y.-J.; Wu, C.-Y.; Li, T.; Hsiao, P.-W.; Chang, D.-K. A Rapid and Sensitive Early Diagnosis of Influenza Virus Subtype via Surface Enhanced Raman Scattering. *Biosens. Bioelectron.* **2014**, *5*, 10001550.
(24) Nguyen, A. H.; Lee, J.; Choi, H. I.; Kwak, H. S.; Sim, S. J. Fabrication of plasmon length-based surface enhanced Raman scattering for multiplex detection on microfluidic device. *Biosens. Bioelectron.* **2015**, *70*, 358−365.
(25) Karn-orachai, K.; Sakamoto, K.; Laocharoensuk, R.; Bamrungsap, S.; Dharakul, T.; Miki, K. SERS-based immunoassay on 2D-arrays of Au@Ag core−shell nanoparticles: influence of the sizes of the SERS probe and sandwich immunocomplex on the sensitivity. *RSC Adv.* **2017**, *7*, 14099.
(26) Kim, K.; Lee, Y. M.; Lee, H. B.; Shin, K. S. Silver-coated Silica beads applicable as core materials of dual-tagging sensors operating via SERS and MEF. *ACS Appl. Mater. Interfaces* **2009**, *1*, 2174−2180.
(27) Oscar, H. W.; Margot, M. E. S.; Kees, O.; Bart, G.; Jan, G.; Peter, H.; Hermann, J. G.; Hansgeorg, S.; Yvette, K.; Carl, G. F. Simultaneous Height and Adhesion Imaging of Antibody-Antigen Interactions by Atomic Force Microscopy. *Biophys. J.* **1998**, *75*, 2220−2228.
(28) Yanagida, S.; Nishiyama, S.; Sakamoto, K.; Fudouzi, H.; Miki, K. Formation of Uniform and High-Coverage Monolayer Colloidal Films of midnanometer-sized gold particles over the entire surfaces of 1.5 in. substrates. *Langmuir* **2017**, *33*, 9954−9960.
(29) Park, Y.-K.; Park, S. Directing close-packing of midnanosized gold nanoparticles at a water/hexane interface. *Chem. Mater.* **2008**, *20*, 2388−2393.
(30) Shankar, C.; Dao, A. T. N.; Singh, P.; Higashimine, K.; Mott, D. M.; Maenosono, S. Chemical stabilization of gold coated silver core-shell nanoparticles via electron transfer. *Nanotechnology* **2012**, *23*, No. 245704.
(31) Karn-orachai, K.; Ngamaroonchote, A. Role of polyelectrolyte multilayers over gold film for selective creatinine detection using Raman spectroscopy. *Appl. Surf. Sci.* **2021**, *546*, No. 149092.
(32) Xie, R.; Karim, A.; Douglas, J. F.; Han, C. C.; Weiss, R. A. Spinodal Dewetting of Thin Polymer Films. *Phys. Rev. Lett.* **1998**, *81*, 1251−1254.
(33) Song, C.; Min, L.; Zhou, N.; Yang, Y.; Su, S.; Huang, W.; Wang, L. Synthesis of Novel Gold Mesoflowers as SERS Tags for Immunoassay with Improved Sensitivity. *Apl. Mater. Interfaces* **2014**, *6*, 21842−21850.
(34) Njoki, P. N.; Lim, I.-I. S.; Mott, D.; Park, H.-Y.; Khan, B.; Mishra, S.; Sujakumar, R.; Luo, J.; Zhong, C.-J. Size Correlation of Optical and Spectroscopic Properties for Gold Nanoparticles. *J. Phys. Chem. C* **2007**, *111*, 14664−14669.
(35) Rev, V.; Kovner, M. A. *Assignments for Vibrational Spectra of Seven Hundred Benzene Derivatives*; Institute of Physics Publishing: Bristol, U.K., 1974.
(36) Wu, W.-T.; Chen, C.-H.; Chiang, C.-Y.; Chau, L.-K. Effect of surface coverage of gold nanoparticles on the refractive index sensitivity in fiber-optics nanoplasmonic sensing. *Sensors* **2018**, *18*, 1759.
(37) Niu, J.; Shin, Y. J.; Son, J.; Lee, Y.; Ahn, J.-H.; Yang, H. Shifting of surface plasmon resonance due to electromagnetic coupling between graphene and Au nanoparticles. *Opt. Express* **2012**, *20*, 19690−19696.
(38) Zeng, Y.; Madsen, S. J.; Yankovich, A. B.; Olsson, E.; Sinclair, R. Comparative electron and photon excitation of localized surface plasmon resonance in lithographic gold arrays for enhanced Raman scattering. *Nanoscale* **2020**, *12*, 23768−23779.
(39) Howanitz, J. H. Immunoassay for Measuring Prostate-Specific Antigen. *Lab. Med.* **1996**, *27*, 255−258.
(40) Delgado, J. C.; Shulman, L. N.; Gudrais, P. G.; Fischer, G. A.; Ferguson, D. O.; Winkelman, J. W.; Tanasijevic, M. J. Standardization of Carcinoembryonic Antigen Testing in the Setting of Clinical Laboratory Consolidation. *Lab. Med.* **2001**, *32*, 92−95.
(41) Steinberg, W. The clinical utility of the CA 19-9 tumor-associated antigen. *Am. J. Gastroenterol.* **1990**, *85*, 350−355.

https://doi.org/10.1021/acs.langmuir.1c01556
Langmuir 2021, 37, 10776−10785